lubricants

MDPI

Article

In Situ Operando Indicator of Dry Friction Squeal

Maël Thévenot [1,*], Jean-François Brunel [1], Florent Brunel [1], Maxence Bigerelle [2], Merten Stender [3], Norbert Hoffmann [4] and Philippe Dufrénoy [1]

[1] Laboratoire de Mécanique Multiphysique Multiéchelle, LaMcube, UMR 9013, Centrale Lille, CNRS, University Lille, 59000 Lille, France; jean-francois.brunel@polytech-lille.fr (J.-F.B.)
[2] LAMIH-Laboratoire d'Automatique de Mécanique et d'Informatique Industrielles et Humaines, UMR 8201, CNRS, University Polytechnique Hauts-de-France, 59313 Valenciennes, France
[3] Mechanical Engineering Group, Berlin University of Technology, 10623 Berlin, Germany; merten.stender@tu-berlin.de
[4] Dynamics Group, Hamburg University of Technology, 21073 Hamburg, Germany; norbert.hoffmann@tuhh.de
* Correspondence: mael.thevenot@univ-lille.fr

Abstract: In various applications, dry friction could induce vibrations. A well-known example is frictional braking systems in ground transportation vehicles involving a sliding contact between a rotating and a stationary part. In such scenarios, the emission of high-intensity noise, commonly known as squeal, can present human health risks based on the noise's intensity, frequency, and occurrences. Despite the importance of squeal in the context of advancing urbanization, the parameters determining its occurrence remain uncertain due to the complexity of the involved phenomena. This study aims to identify a relevant operando indicator for predicting squeal occurrences. To this end, a pin-on-disc test rig was developed to replicate various contact conditions found in road profiles and investigate resulting squealing. Each test involves a multimodal instrumentation, complemented by surface observations. It is illustrated that the enhanced thermal indicator identified is relevant because it is sensitive to the thermomechanical and tribological phenomena involved in squealing.

Keywords: brake squeal; thermal solicitation; surface topography; friction-induced vibrations; tribology

Citation: Thévenot, M.; Brunel, J.-F.; Brunel, F.; Bigerelle, M.; Stender, M.; Hoffmann, N.; Dufrénoy, P. In Situ Operando Indicator of Dry Friction Squeal. *Lubricants* **2024**, *12*, 435. https://doi.org/10.3390/lubricants12120435

Received: 9 October 2024
Revised: 4 December 2024
Accepted: 6 December 2024
Published: 8 December 2024

1. Introduction

Braking function is a critical element in any vehicle. Whereas various braking technologies are in use, friction braking still remains the most prevalent. It is considered as the most effective and reliable, which is of particular interest for a component used in emergency situations. Particular attention has been paid over the years to the development of these braking systems, which realize this conversion of the vehicle's kinetic energy into other forms, primarily heat, as the brake pads interact with the brake disc. However, the use of friction brakes still involves significant unresolved problems. Thus, friction instabilities, thermal fatigue [1], wear [2] and particles or noise emissions such as squealing [3] remain as significant challenges to the improvement of these systems. The occurrence of brake squeal in vehicles is one of the most expensive issues in industrial applications (after-market) [4], and significant efforts are made to mitigate this [5]. It is a particularly problematic issue for people, due to its high frequency and acoustic pressure (above 1 kHz and starting at 70 dB). This challenge is all the more true for electric vehicles, which are even more sensitive to noise due to the absence of noise-covering combustion engine sounds. It is commonly accepted that squealing comes from self-excited vibrations of the brake system, which endure unstable dynamical behavior (like mode coupling) under sliding frictional contact conditions [6]. But a complete understanding of its physics is still lacking, as it remains a complex phenomenon affected by multiple factors on multiple scales from the behavior of structural components to external excitations, as well as the dynamics of the friction interface during braking.

Over the years, to enhance our understanding of the mechanisms leading to squeal events, researchers have conducted experiments and numerical studies to investigate the behavior of the contact interface. Experimental studies shown that within a sliding contact, the evolution of imposed conditions [7,8] and macroscopic aspects [9], such as changes in the friction material, surface's geometry and tribolayer (thin film at the interface) are interconnected and have an influence on the squeal occurrence [10]. Different rotation speeds of the rotating part, for example, lead to the evolution of vibration responses and contact behaviors. Relationships can be observed, such as a stronger vibration response occurring at lower disc rotation speed, like 200 rpm, leading to high sound pressure level [11] and also severe localized wear and rough pad surface. Moreover, research works reported a strong correlation between wear and squeal occurrence in braking systems [12]. From prepared parts [13], successive contacts gradually modify the contact behavior with an elevation of the friction coefficient until it starts to plateau around a critical value. Squeal occurrence sharply increases once this contact behavior is reached, coinciding with increased use of parts. However, it has been observed that the friction coefficient and its variation are not enough to explain squeal occurrence, as many studies address the fact that mode coupling can take place under a constant friction coefficient. This coefficient should rather be viewed as a response of the tribological system. Finite element models employing complex eigenvalue analysis (CEA) have also demonstrated the sensitivity of components (dynamic modes) and system parameters (assembly with connections) on squeal propensity [14]. The influence of thermomechanics and friction materials on the dynamic response has also been highlighted [15,16]. However, the models are still not predictive.

Additional studies focused on the evolution of friction material and tribology [17], demonstrating the complexity of involved mechanisms, as the friction material undergoes modifications due to thermal, mechanical and tribological loading as far as the tribolayer. On both mesoscopic (contact geometry) and microscopic (particles flow) scales, it is known from the third-body approach proposed by Godet [18] and Berthier [19] that the flows and compaction of worn particles (which constitute the major part of what is called the third body) play a crucial role in the creation of the tribological surface layers [20]. These changes at a microscopic scale such as evolution of the contact surface heterogeneity (due to material degradation and presence of a third body) significantly impact squeal occurrence. This is interconnected with the tribological circuit and its complex behavior [21]. It has been shown that without changes to the interface (no wear of friction material, and hence no third body in the contact and constant macro contact surface), a tribological system remains silent and squeal only occurs upon the addition of a third body. Squeal occurrence is then highly dependent of the size and nature of particles flowing through the contact [22], in addition to the rest of the contact conditions (friction coefficient, dissipated energy, etc.). Numerical works also show that the emergence of squeal is dependent on the evolution of the surface and material transformation beneath the surface of friction material [23].

Most recent experimental studies addressing squeal issues and tribology in general tend to include the observation of the worn surface after contact [24]. The added value of these observations is, however, often limited, as after opening the contact, a significant amount of critical information is lost, particularly if the observation requires a lot of manipulation of the parts. The distribution of contact plateaus in the tribolayer, which are formed by hard ingredients and wear debris compaction around them, have been shown to have an influence on squealing events [25]. The impact of the changes in the actual contact localization at macro and meso scales on the squealing frequencies of a pin-on-disc system have also been highlighted [26]. This research work emphasizes how the evolution of the contact state during dry friction significantly influences the squeal occurrence. However, the contact is not accessible during contact, which makes characterizing its state only feasible before and after the tests. Therefore, it would be very useful to have an indicator to identify the conditions in which squeals emerge, in order to anticipate how to avoid them. In this work, we propose to explore indicators other than global ones, such as friction

coefficient or disc temperature, which are often linked, but only partially correlated with squeal noise. To this end, the indicator must be related to the phenomena described above, hence the idea of a carefully chosen intrusive measurement. Thermomechanical constraints on the friction material are monitored during tests with embedded thermocouples and Foucault's displacement sensors, while a microphone records the noise. A discrete tracking of the friction material surface with a remote head profilometer is introduced, allowing for optical observations as well as profilometry without disassembling the parts.

2. Methods

2.1. Experimental Setup

For this study, a pin-on-disc (PoD) tribometer developed for another study [9] was adapted to perform the required test conditions (Figure 1). The interest of this set-up is to master the dynamic behavior of the system by the limited assembly. It is made of a rigid stand on which an aluminum blade is attached to its extremities. The pin is glued at the center of the blade. The imposed displacement of the rigid frame with a motorized table along the axial disc direction pushes the pin against the disc and the bending of the blade gives the normal load, as detailed in Section 2.3.

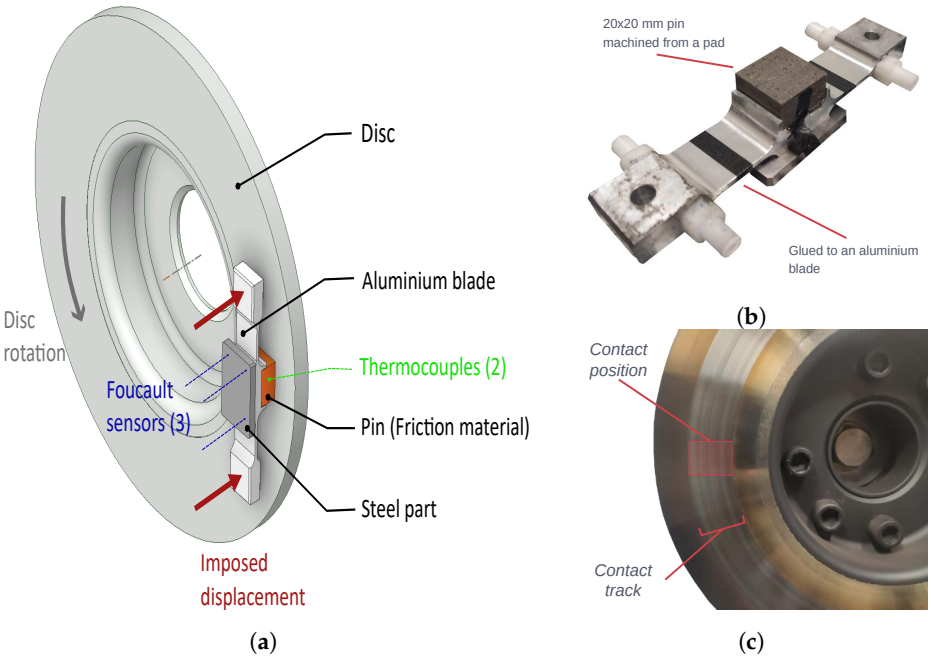

Figure 1. (**a**) Schematic representation of parts in contact. (**b**) Stationary part: pin of friction material mounted on aluminum blade. (**c**) Rotating part: steel disc with contact location.

The 20 × 20 mm pin is machined from a complete pad, with a height of 10 mm. A diamond disc polisher is used to ensure the dimensions of the pin. The disc has an external diameter of ∅220 mm and the mean contact radius on the disc is set at 100 mm, as illustrated in Figure 1. Materials used for this study are detailed in Section 2.4.

2.2. Testing Conditions

The test campaign is divided into series of 20 successive friction tests with fixed conditions, including contact and non-contact conditions. Friction tests are performed with a constant disc rotation speed and an imposed displacement to obtain the desired normal load at the start of the test. The rigid frame position is then kept constant during all the test series, leading to a variation of the normal load due to thermomechanical solicitations (thermal dilatation and wear).

Different test configurations can be achieved by modifying the desired normal load (200 N, 400 N), the disc rotation (200 rpm, 600 rpm, 700 rpm), the contact duration (10 s,

30 s) or the non-contact duration between successive tests (5 s, 10 s, 30 s). The reduction in the non-contact duration leads to a higher temperature elevation of the disc and the pin. This approach allows us to perform a large number of tests; for this test campaign a reduced combination of solicitations have been explored, which allowed us to repeat them a large number of times.

Figure 2 presents the test conditions investigated through the whole campaign. Disc rotation speed is represented, as well as the pin's axial starting position through the campaign. Its position is updated when necessary to ensure that a fixed displacement led to the desired normal load at the beginning of each test series (200/300 N). The global evolution of the pin's axial position through the campaign demonstrates the wear of the pin. Duration during (ON) and between (OFF) each of the tests is also indicated. Finally, between each test series, a red dot on the line of the disc's rotating speed corresponds to instants where an optical observation of the pin's surface is performed.

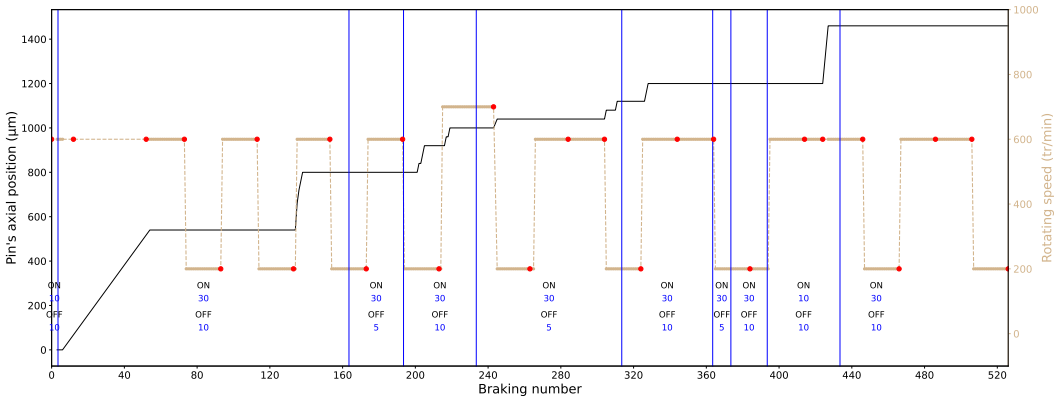

Figure 2. Test conditions investigated in this study in terms of rotation speed of the disc and pin's axial displacement. Duration of test (ON) and between each test (OFF) are indicated in blue in seconds and pin's surface observations with red dots.

2.3. Instrumentation

A dedicated instrumentation has been implemented to characterize thermomechanical constraints during the contact process.

Three Foucault displacement sensors measure the aluminum blade's bending. Knowing the blade's stiffness, from those sensors, the contact normal load is obtained. This relationship between displacement and force is obtained by prior calibration. Two type K thermocouples with a diameter of ∅1 mm are inserted in the pin, located 2 mm below its surface. Both thermocouples are in the same radial position (regarding the disc), one toward the leading edge (TC1) and the other toward the trailing edge of the contact (TC2), as illustrated in Figure 3. Sound from the tests is recorded using a microphone, the range of which is from 3 Hz to 20 kHz. It is located at a distance of 1 m from the disc. Mechanical sensors and microphone signals are recorded using an high rate acquisition sampling rate of 50 kHz, while thermocouples are recorded at a sampling rate of 90 Hz.

Lastly, a profilometer (Alicona, PortableRL model) is integrated into the test bench to conduct discrete tracking of the pin's surface. Based on the technology of focus variation, it can provide information regarding topography. Its white-light lighting allows fixed observation conditions through a test campaign, to be able to compare images taken with fixed settings. For this purpose, the steel frame holding the pin's blade can be rotated to two predefined target positions: either in a test configuration to perform contacts (pin in front of disc) or in an observation configuration (pin in front of profilometer). Mechanical clamping for these target positions ensures that they remain the same throughout the campaign. Figure 3 illustrates the pin's placement in both configurations, with indications of the thermocouple positions. The pin's surface is examined through a 4× objective with a vertical resolution of 1.4 µm and a lateral resolution of 7 µm, using stitching techniques to enable an image of the whole pin surface to be obtained (25 stitches to cover the 20 × 20 mm surface).

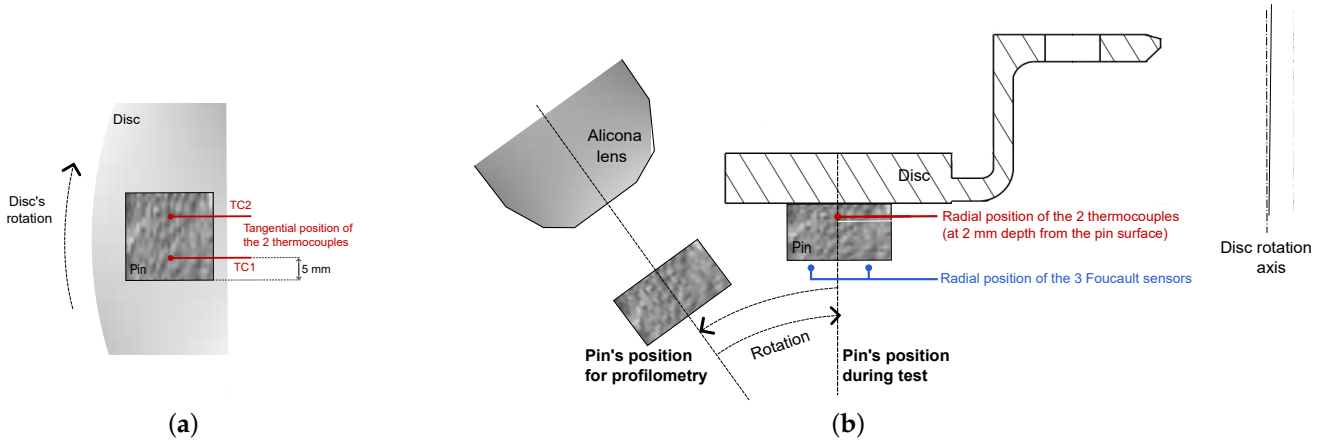

Figure 3. (**a**) Top view of the test bench presenting the pin's positions for test and observation. (**b**) Front view of the pin in testing position.

2.4. Materials

A disc made of steel and a commercial low-met friction pad material designed for railway applications are used. As this material is used in industry, its formulation is only partially known, without details about raw components or process (except that the maximum processing temperature is 200 °C, and that the surface undergoes grinding without subsequent polishing). SEM observations have been conducted of the material before tests to have a better understanding of its composition. Some components have been identified either through EDX analysis or due to their particular shape. The material demonstrates a matrix made of resin and rubber, with metallic fibers. The friction surface is taken as if it is on pads, i.e., after machining by material removal.

An optical observation of the pin's surface is realized before the test campaign with the profilometer, as shown in Figure 4a. At this macroscopic scale, the material presents a high degree of heterogeneity. Patterns of different colors with a size around 3 to 4 mm are observed. Some are darker and others are brighter with an orange tint.

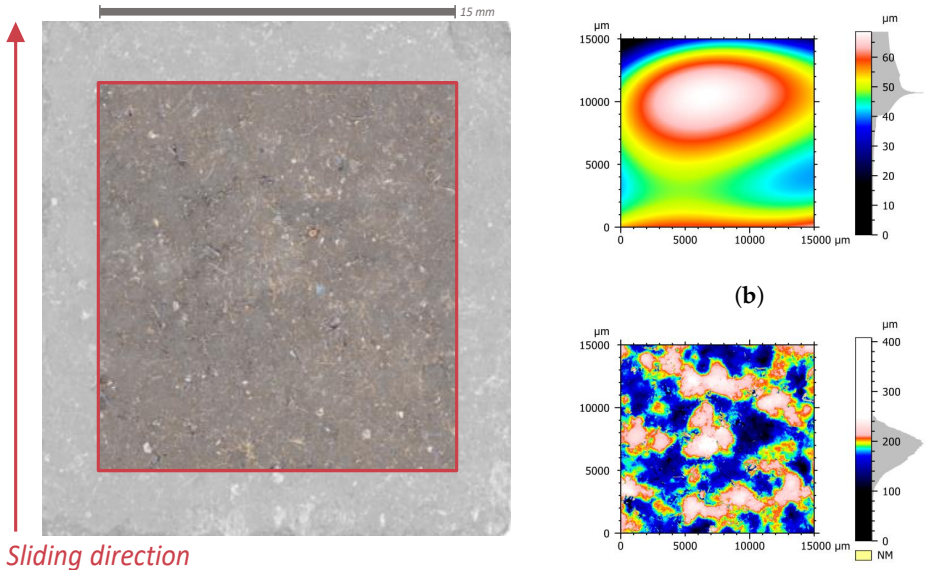

Figure 4. Profilometry observation of the pin before tests. (**a**) Image of the 20 mm × 20 mm pin's surface, with some brighter patterns highlighted. (**b**) Shape of the pin's surface. (**c**) Pin's profilometry without the shape.

In addition to the optical observation, the profilometer allows us to obtain the topography of the pin's surface. To correctly investigate the pin's profilometry, a pre-processing of the data is carried out. First, aberrant or unmeasured points are removed. A windowing operation is then performed to retain only a region of 15 mm by 15 mm centered at the center of the pin (highlighted center area in Figure 4a). This allows us to remove the edges from further operations. A straightening operation is then carried out by removing a least squares plane from the surface. Finally, the shape is removed from the image with a third-degree polynomial (Figure 4b). The resulting surface (Figure 4c) contains the waviness and roughness, without the global shape of the pin. In this surface, patterns with the same scale as those noticed on the image are visible with a difference in terms of height compared to the rest of the surface. It confirms a strong heterogeneity at a millimeter scale (around 3–4 mm), probably due to the formulation and processing of the material.

3. Results

3.1. Global Results

Figure 5 presents the thermal and mechanical measurements along the campaign. For each test, the maximum normal load and the maximum temperature for the two thermocouples are shown. Disc rotation speed is still represented to facilitate the comparison with Figure 2. Each test series is visible on the pin temperatures, which rise during the series. Depending on the imposed normal load, contact duration and rotating speed of the disc, the temperature rises are different during the cycle. Overall, the thermocouple at the trailing edge (TC2) displays higher temperatures than the thermocouple at the leading edge (TC1) of the contact. It should be noted that the TC2 was detached during one series (from test 425 to 445). For the majority of the test campaign, maximal temperatures are correlated with maximal normal load elevation, with the exception of the first temperature rise above 200 °C, where the normal load decreased during temperature elevation. Enduring high thermal solicitations, pin materials may have undergone transformations.

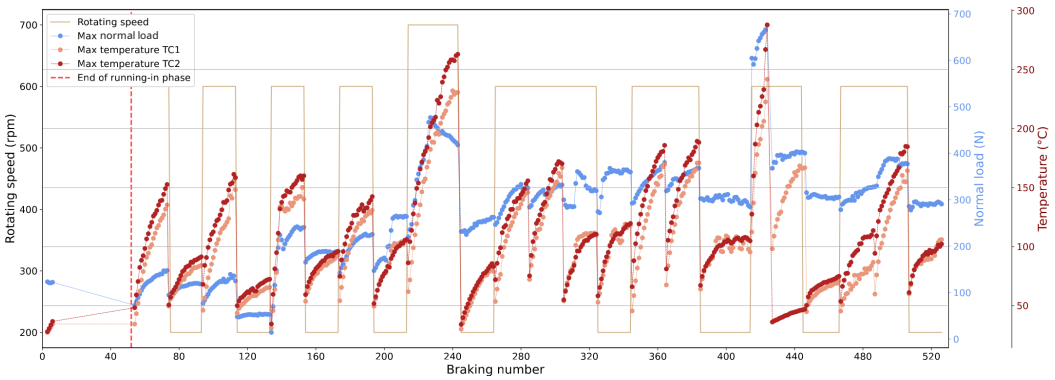

Figure 5. Thermomechanical conditions investigated, resulting from the imposed test conditions.

3.2. Surface Analysis

Besides the continuous measurements of thermomechanical constraints performed during tests, discrete tracking of the pin surface is achieved through optical and profilometry measurements. Those observations allow us to track the evolution of the surface state before and after each cycle of tests. Comparing the images allows us to track some material flows, such as the appearance or ejection of particles, as well as changes in the powder deposited on the surface, whereas profilometry gives an evolution of the topography of the pin surface through the campaign. Profilometry observation before tests showed a pattern on the pin's surface, with significant amplitude variations every 3–4 mm. In order to track their evolution through the campaign, it is necessary to have a quantitative indicator of these patterns. Surfaces from which shape is removed, thanks to the previously presented post-processing, allow us to calculate a range of surface roughness parameters to characterize certain aspects of the surface. First, a certain cut-off needs to be chosen to determine at

which scale the surface is characterized, then roughness parameters can be calculated for each surface. A statistical analysis (MESRUG) was performed to compare the relevance of roughness parameters regarding the surface state [27]. Among the various calculated roughness parameters, S5p with a specific cut-off of 4413 µm using a non Gaussian filter emerged as the most representative parameter for capturing the evolution of observed patterns. Figure 6 represents the S5p of each profilometry observation of the campaign.

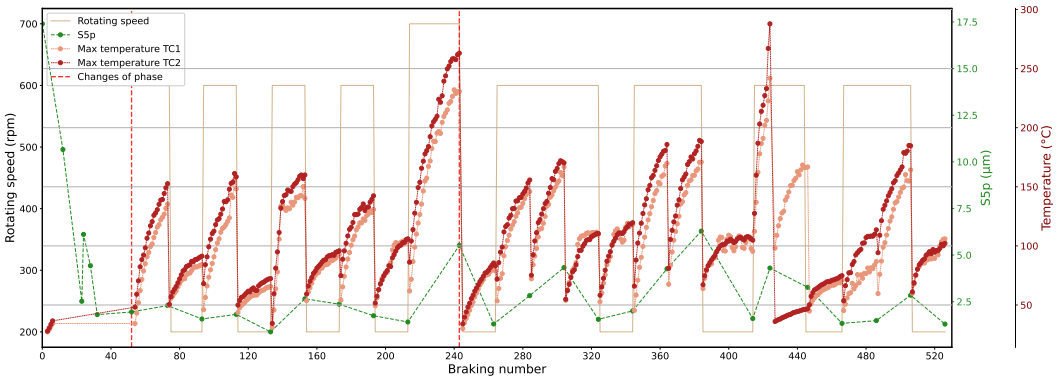

Figure 6. Evolution of the surface roughness parameter S5p during the test campaign.

There is a quick decrease in the S5p during the first 40–50 tests of the campaign. It is related to the running-in phase at the beginning of the test campaign, during which there is a rise in the macroscopic load-bearing area between the parts until the contact occurs across the entire pin surface. After 50 tests, the optical observation showed that the contact front went through the entire pin surface, and the running-in phase is considered complete. The characterization of the surface through this roughness parameter highlights the change in amplitude on the surface during the running-in phase, due to the erosion of the initial peaks. The S5p stabilizes with the evolution of test series conditions; most energetic tests induce an increase in the parameter, and vice versa. During the first 210 tests, the S5p at this scale does not show much variation. Then, the cycle with the first rise in temperature above 200 °C that the pin endures is realized. During this cycle, an important variation of the S5p is observed. For the rest of the campaign, the S5p continues to show a lot more variation when the pin's temperature rises. During these tests, the material roughness at the observed scale provides some insights into past thermal conditions.

Regarding the pattern amplitude on the topographies, it appears that some surfaces present a lot of similarities to each other, in correlation with the S5p parameter. To investigate phenomena and solicitations responsible for those changes in the surface, topographies were grouped together in classes according to the similarity of the pattern. Four distinct classes could be established (Figure 7). Class A is characteristic of the pin's state before tests and is never observed again during the campaign (high value of S5p). During the rest of the campaign, the three other classes appear one after another regarding the test conditions (Figure 8; two images are marked "unmeasurable", as the measured images were incomplete). In general, higher temperature levels lead to surfaces that fall in class B (medium value of S5p), while lower constraints lead to surfaces in class D (with class C in between, with a low value of S5p). To have a better understanding of those resulting topographies, images of the surfaces are shown in Figure 7 as well. On the surfaces, some powdery matter is observed (dark color in asperities on the images). It is identified as a powdery third body that flows through the contact during the test, and can be trapped in asperities and porosities of the surface, and sometimes accumulate enough to participate in the contact, showing compaction. For all images, the more powdery matter is present on the surface, the more the surface falls into class D (surfaces A and B showing less powder).

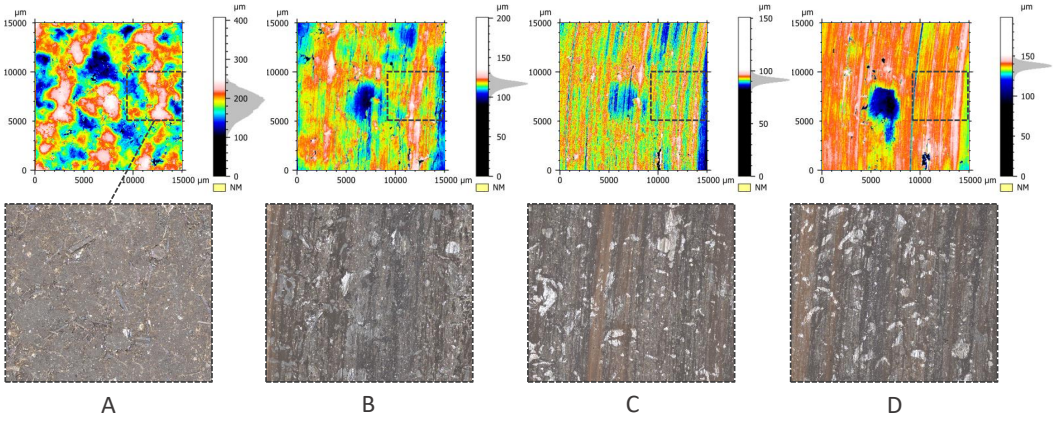

Figure 7. Classes of surface topography observed with a zoomed area of each corresponding image: (**A**) very rough aspect, (**B**) rough with a noticeable friction direction, (**C**) clear sliding direction and smaller high differences, (**D**) rather smooth surface with a local porosity.

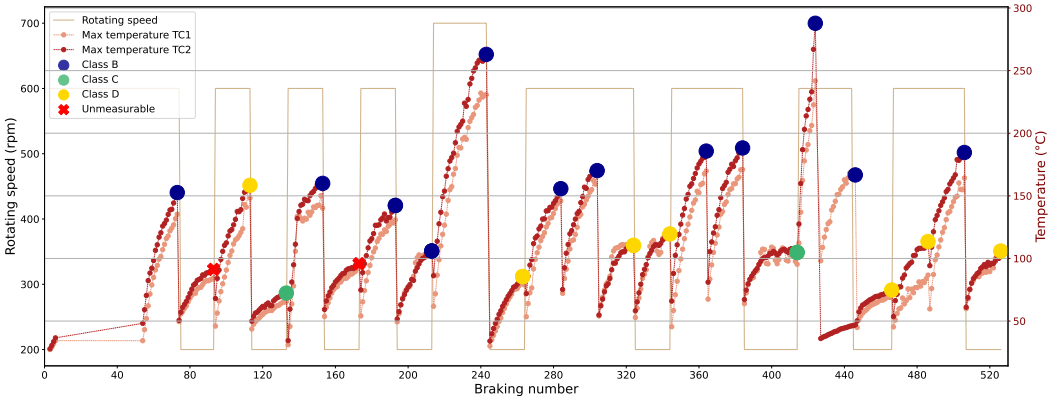

Figure 8. Classification of the profilometry observations through the test campaign.

Surface observations highlighted a link between tribological circuit and solicitations. Contact conditions inducing lower thermal solicitations on the parts increases the storage capacity of powder within the interface. The contact area appears more enclosed when thermal phenomena are limited. This inclination to favor powder storage at the interface leads to the filling of surface irregularities, resulting in a smoothing effect (and a lower S5p). Higher thermal solicitations result in rougher surfaces and emptier asperities. Intense thermal phenomena lead to more pronounced opening of the interface and facilitate particle ejection. Squeal phenomena are associated with variations in the effective contact area between components. The impact of these surface state variations under different thermal solicitations on squeal occurrence will now be investigated.

3.3. Noise Emission Analysis

In this paper, noise emissions are considered as squeal when the threshold of 70 dB is reached for any frequency. The frequency range of concern spans from 1000 Hz (excluding bench noise) to 20 kHz. Figure 9 provides an overview of the campaign with the squealing frequency of highest intensity and its harmonics for each test. To process the signal from the microphone, which has a 50 kHz sampling frequency, a Short-Time Fourier Transform is applied to obtain the acoustic spectrogram.

The disc's rotation speed is presented as well. Different frequencies are obtained with the presence of harmonics which are characteristic of squeal. As seen before with the surfaces, different phases of the campaign result in changes in the noise emission. Most of the silent tests occur at the beginning of the campaign, where the normal load is low and the contact area evolves a lot during each test or during the beginning of each test series.

During the first phase of the campaign up to brake number 210, only one squeal frequency at 2.1 kHz (with its harmonics) is obtained, which appears to be sensitive to the test conditions. During the high-temperature series, high thermal solicitations lead to a new squeal frequency (5.3 kHz). This squeal frequency is then obtained for each test series where the temperature is high. At low temperature, two other frequencies are observed (3.3 kHz and 18 kHz). The three first low frequencies are very close to the disc's natural frequency [26]. It should be noted that the frequency at 2.1 kHz no longer appears after the first high-temperature test series, which may be related to a strong transformation of the contact interface and certainly of the friction material near the surface.

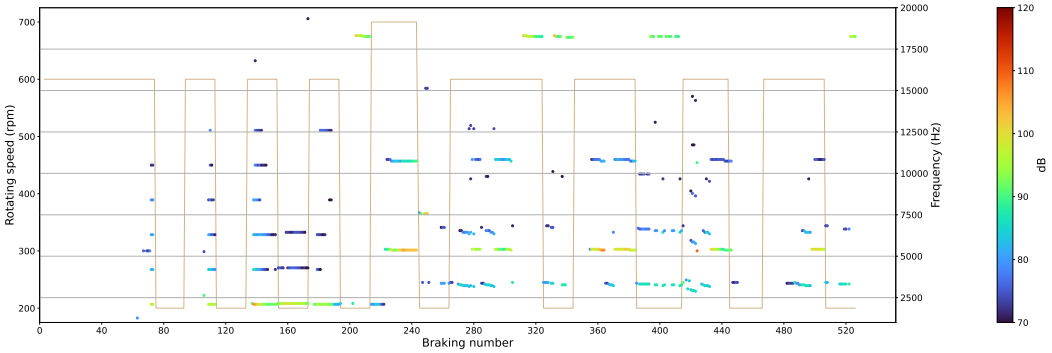

Figure 9. Overall acoustic results during the campaign: squeal detection for each frequency > 70 dB, disc's rotating speed and maximal temperature of the pin.

To highlight the main squeals of this campaign of more than 500 tests, a classification of the different obtainable spectrograms has been performed. Similar to what was performed for the surface, the idea is to identify the mechanisms responsible for the main behavior that emerges. For the whole test campaign, the harmonics are removed and a +/−500 Hz window gathers close squealing frequencies together. It results in only four different fundamental squealing frequencies. Each of these frequencies was associated with a squealing class for the classification (plus a class corresponding to an absence of squeal). Figure 10 presents some examples of spectrograms obtained during the individual test, associated with each identified squeal class. This classification is rather simple, so the duration of the squeal is not taken into account (as long as the frequency is above 70 dB for at least 1 s, it is classified in the corresponding category), and if multiple of those squealing frequencies appear in one test, it is added to all the corresponding classes.

Figure 11 resumes the spectrogram classes through the campaign. It can be noted that some tests fall in multiple classes. It is observed that classes No Squeal and 2.1 kHz Squeal are mostly observed before the transformation cycle occurring at test 215, and at rather low solicitations for class No Squeal. For the rest of the campaign, the previously observed correlation with the maximal temperature of the pin appear even more clearly. Class 5.3 kHz Squeal is the only frequency observed when the pin's temperature is above 140 °C, whereas at lower temperatures, behaviors appear more complex. Multiple squeal frequencies share the same range of temperature as classes 3.3 kHz Squeal and 18 kHz Squeal are observed. So the level of temperature seems to be a strong indicator, especially for the triggered squeal frequency at high temperatures. On the other hand, temperature variations allow us to make the distinction between some squealing frequencies at low temperature levels. When the squealing class 18 kHz Squeal occurs, the temperature fluctuates around a constant level, and the temperature of the TC1 thermocouple is higher than the temperature of the TC2, contrary to the squealing class 3.3 kHz Squeal, which appears only during temperature rises, with maximum temperature at the TC2. So the temperature is, for this test setup, a discriminating indicator for squeal frequencies, and beyond the temperature level, the heat kinetics and distribution are also important factors.

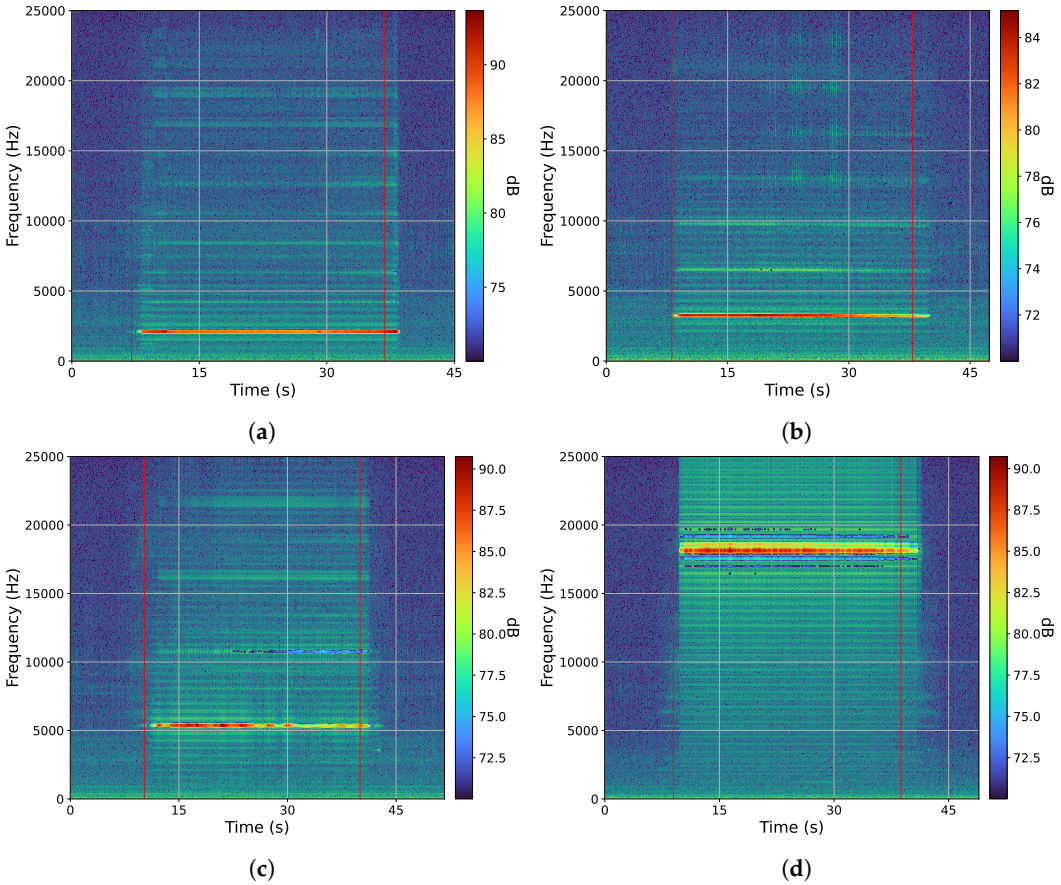

Figure 10. Classification of noise emissions for individual test. (**a**) 2.1 kHz squeal, (**b**) 3.3 kHz squeal, (**c**) 5.3 kHz squeal, (**d**) 18 kHz squeal.

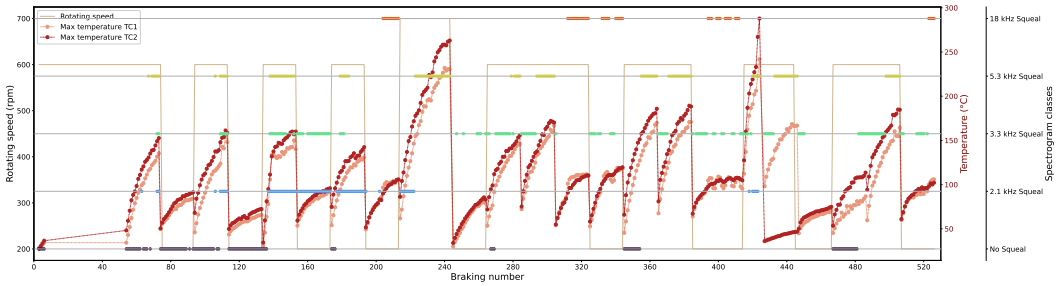

Figure 11. Classes of noise emissions observed for each test through the campaign, with rotating speed of the disc and pin temperature.

4. Discussion

Figure 12 presents an overview of all frequency classes, regarding the max temperature of the pin (maximum of the two thermocouples) in the last test performed just before the profilometry acquisition. The surface class is also indicated to compare with squeal classification. Class *A* for initial state has been removed here, and points circled in the gray tinted area correspond to observations realized before the transformation cycle with high thermal solicitation (test 0 to 215). As seen before, surfaces with topography of class *B* are only obtained if the pin temperature previously reached more than 140 °C. And those tests only correspond to squeal class *2.1 kHz Squeal* during the running-in phase, or *5.3 kHz Squeal* for the rest of the campaign. Below 140 °C, behavior appears more complex. Surface class *D* seems to occur most of the time for the lower temperature, but there is an overlap in term of temperature with the surface *C*, which is also present around 110/120 °C. A connection is highlighted between maximum pin temperature, squeal classes and surface classes.

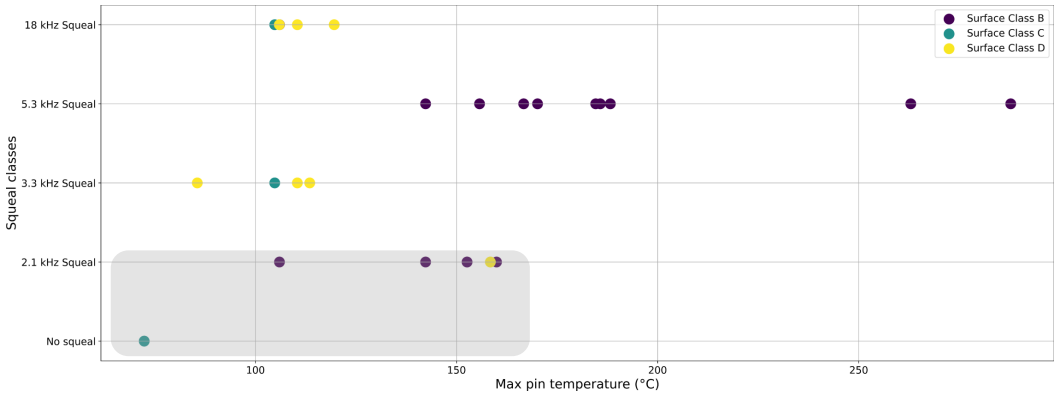

Figure 12. Representation of frequency classes regarding maximum temperature of the pin, with surface classes for corresponding profilometry observation.

Relationships have been established here between surface and squeal classes regarding the temperature solicitation, but only considering the maximum pin temperature of the test before profilometry. Yet, the profilometry observations are relatively scarce in comparison to the number of tests performed and the temperature level reached alone does not suffice to indicate squeal frequencies at lower temperatures. As mentioned before, temperature variations and heat kinetics on the surface area must also be considered to differentiate noise emissions. The impact of a test cycle reaching temperatures sufficient to potentially alter the material of the pin must also be acknowledged. The strong correlation between maximum temperatures and the pin surface state take places after this intense thermal solicitation.

A more in-depth analysis of the thermal solicitation on squeal for tests after the transformation cycle (tests 240 to 526) is presented in Figure 13. The maximum difference of temperature between the two thermocouples is displayed (trailing edge minus leading edge thermocouple) regarding the maximum reached temperature. All resulting points are connected to the centroïd (center of mass represented by a triangle) of their respective point clouds, which have the convex hull of their area colored for a better visualization. For this representation, squeal class *2.1 kHz Squeal* is excluded due to its limited number of data points. The number of displayed tests is still more substantial than the number of profilometry observations, allowing for the verification of previously observed hypotheses across a larger sample group.

As previously noted, the maximum pin temperature remains a distinguishing factor for class *5.3 kHz Squeal*, with only a few tests of class *3.3 kHz Squeal* falling within the same temperature range. Some of these few tests of class *3.3 kHz Squeal* showing a maximum pin temperature above 150 °C correspond to tests 417 to 419, which takes place in a high-temperature test series with potential material transformations being able to impact squeal frequency. The rest of these tests correspond to tests 496 and 497, where a squeal at 3.3 kHz occurs only at the beginning of the test and disappears when the temperature rises. So those points should in reality be linked with a lower temperature than the maximum pin temperature reached during the whole test. A more precise classification of squeal frequency regarding pin temperature would allow for an even more clear discrimination of temperature domains of each squealing frequency.

At lower temperatures, although classes *No Squeal*, *3.3 kHz Squeal* and *18 kHz Squeal* share a similar range of maximum pin temperature, clear differences emerge in terms of the temperature gap between the two thermocouples. Class *18 kHz Squeal* in particular is clearly delineated on this graph, appearing from 100 °C and only for low or negative temperature differences. While, in the majority of tests, the thermocouple at the trailing edge reaches higher temperatures, for some tests, the one at the leading edge of the contact exhibits higher temperature, triggering this particular frequency. This variation in temperature differences can be associated with an uneven distribution of contact pressure, which indicates a change in the load bearing. This change in bearing capacity may itself be

linked to thermomechanical effects (e.g., dilatation) or interface variations (tribolayer or material detachment).

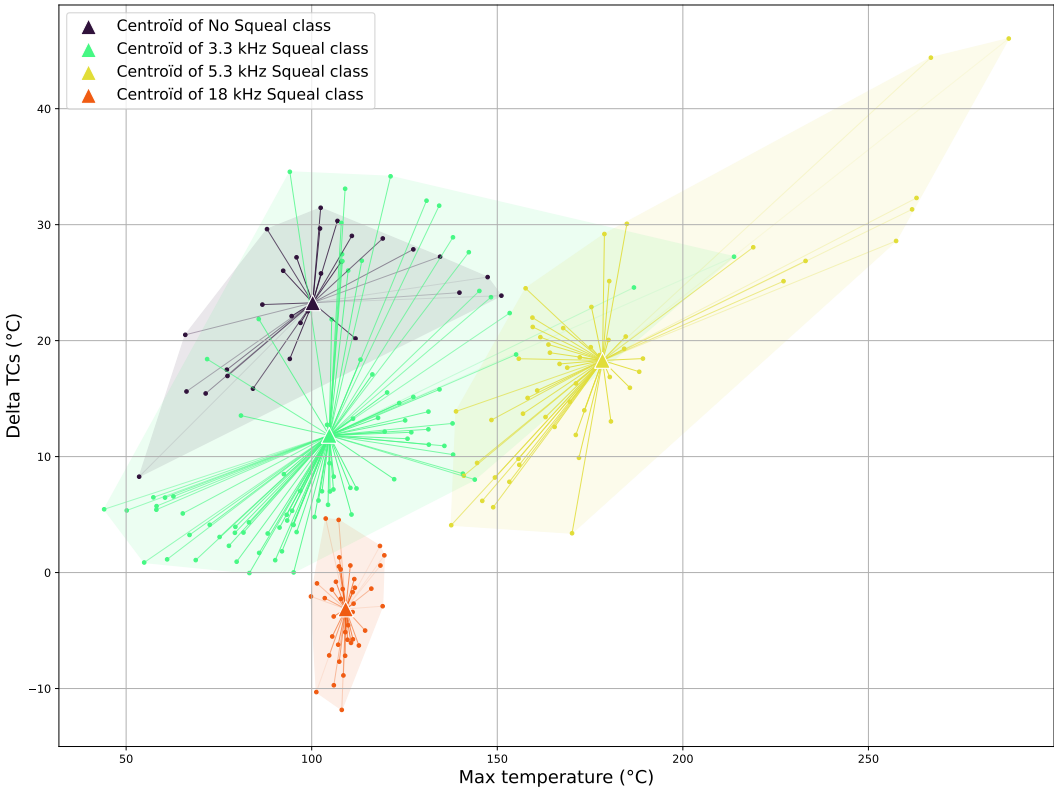

Figure 13. Temperature difference of pin thermocouples for tests 240 to 526, regarding the maximal pin temperature.

In contrast, the absence of squealing (class *No Squeal*) is noted between 50 °C and 150 °C, but only when the thermocouple at the trailing edge records significantly higher temperatures than its counterpart. Class *3.3 kHz Squeal* displays the widest range in both maximum pin temperature and temperature differences. However, in most tests where this frequency is triggered, the temperature rise at the trailing edge exceeds that at the leading edge by a margin of around 10 degrees. In this representation, classes *No Squeal* and *3.3 kHz Squeal* still overlap, yet their centroids suggest that a load-bearing area predominantly located on one side of the surface (specifically, at the trailing edge of the contact) tends to favor the absence of squealing. In this configuration, the exit of the contact is more confined, and the internal flow of particles through the contact might be limited if they are mostly emitted near the exit of the contact.

The present study has highlighted a significant correlation between pin temperature and squeal occurrence during dry sliding contacts. This finding aligns with previous research emphasizing the crucial role of temperature in tribological phenomena associated with these events. Investigation of the pin's profilometry has shown a robust correlation between the maximum pin temperature and the resulting surface condition. This suggests that the temperature seen by the material is a main contributing factor to the surface state of the pin. Through the imagery of the profilometry, it appears that the behavior of the third body through the contact and its ability to resorb asperities of the surface, hence lowering its macroscopic roughness, is significantly impacted by the temperature. These results have been confirmed by other experiments on the same device. An extension to other systems would require further investigation, similar to those proposed here, i.e., extended instrumentation for temperature measurement to obtain information on contact localizations. These localizations depend on the rigidity of the system, as does the vibratory response.

Lower-temperatures solicitations allow for a more powdery third body to be trapped in asperities, reducing surface roughness parameters on a scale of several millimeters. It might result in more opportunities for the load-bearing area to evolve as powdery material accumulates or is compacted, thereby triggering a greater variety of squealing frequencies. Conversely, higher thermal solicitations lead to the clearing of asperities and porosities, amplifying the role of millimetric patterns on the surface in contact localization and resulting in more specific and stable squealing frequency. Monitoring the pin's temperature during tests could potentially allow some squealing frequencies to be entirely avoided.

5. Conclusions

The complexity of the phenomena involved in squeal noise explains why, despite the huge amount of work dedicated to this issue, predicting them remains a challenge. It was proposed in this work to identify whether a physical indicator could be obtained to predict squeal situations. It was shown that an operando thermal measurement could enable this prediction. The relevance of this measurement is explained by the links with the physical phenomena influencing squeal, i.e., macroscopic and microscopic contact in relation to thermomechanics and tribology. It appears that variations in these phenomena can be captured by subsurface thermal measurement. However, the complexity of these phenomena can make measurements tricky because it is both far from the surface and relatively simple. It has been shown that a prediction of squeal is achievable by processing both the temperature level and the temperature difference between two measurements located in front of and behind the direction of sliding, provided that the loading history is considered, in particular the high-temperature events which transform the pad material. Discrete surface analysis has shown that the temperature level affects the tribolayer and the difference between the measurements affects the macroscopic load-bearing variation. This type of indicator seems to be able to reflect the intricate mechanisms governing brake system behavior.

Different improvements can be suggested as future work. In-depth processing of squealing events and frequency classification could explain at least in part the overlaps of the fields observed in Figure 13. The number of sensors could be increased, particularly thermal, to access finer location information. Data processing is an important area of improvement, whether by adding information from sensors other than thermal or by using more systematic processing such as machine learning methods, or even by extended processing of measurements to go back to surface information (inverse models). Finally, while, in this study, the focus has been placed on the pin, extensive observation of the disc's surface would be necessary to have a more complete comprehension of the contact behavior.

Various applications could be found for this work. The insights derived from this study could inform the development of strategies to mitigate squeal occurrences by addressing factors such as temperature mitigation. Conditions of brake use that are conducive to squeal could be defined and avoided, for example, with the design of the brake or with the combination of other brakes, such as regenerative brakes.

Author Contributions: M.T. conducted the experiments, analyzed the results, and wrote the manuscript. J.-F.B. conceived the experiment and participated in the writing process. F.B. developed the test bench control and data acquisition system. P.D. contributed to the concept and the methodology of the research, led the project, and participated in the writing process. M.B. assisted with surface analysis. M.S. assisted with data analysis. N.H. contributed to the concept and the methodology of the research and led the project. All authors have read and agreed to the published version of the manuscript.

Funding: This work was carried out as part of the Franco-German PI-CUBE project financed by the BMBF-DFG and MESRI-ANR institutions. It has also been supported by the RITMEA project, which is co-financed by the European Union with the European Regional Development Fund, the French state and the Hauts de France Region Council.

Data Availability Statement: The data generated during and/or analyzed during the study are available from the corresponding author upon reasonable request.

Conflicts of Interest: The authors declare no competing interests.

References

1. Mackin, T.J.; Noe, S.C.; Ball, K.J.; Bedell, B.C.; Bim-Merle, D.P.; Bingaman, M.C.; Bomleny, D.M.; Chemlir, G.J.; Clayton, D.B.; Evans, H.A.; et al. Thermal cracking in disc brakes. *Eng. Fail. Anal.* **2002**, *9*, 63–76. [CrossRef]
2. Österle, W.; Dörfel, I.; Prietzel, C.; Rooch, H.; Cristol-Bulthé, A.L.; Degallaix, G.; Desplanques, Y. A comprehensive microscopic study of third body formation at the interface between a brake pad and brake disc during the final stage of a pin-on-disc test. *Wear* **2009**, *267*, 781–788. [CrossRef]
3. Massi, F.; Berthier, Y.; Baillet, L. Contact surface topography and system dynamics of brake squeal. *Wear* **2008**, *265*, 1784–1792. [CrossRef]
4. Kinkaid, N.M.; O'Reilly, O.M.; Papadopoulos, P. Automotive disc brake squeal. *J. Sound Vib.* **2003**, *267*, 105–166. [CrossRef]
5. Akay, A. Acoustics of friction. *J. Acoust. Soc. Am.* **2002**, *111*, 1525–1548. [CrossRef]
6. Hoffmann, N.; Fischer, M.; Allgaier, R.; Gaul, L. A minimal model for studying properties of the mode-coupling type instability in friction induced oscillations. *Mech. Res. Commun.* **2002**, *29*, 197–205. [CrossRef]
7. Eriksson, M.; Jacobson, S. Friction behaviour and squeal generation of disc brakes at low speeds. *Proc. Inst. Mech. Eng. Part D J. Automob. Eng.* **2001**, *215*, 1245–1256. [CrossRef]
8. James, S.; Ouyang, H.; Brookfield, D.J.; Mottershead, J.E. Disc Brake Squeal—An Experimental Approach. *Mater. Sci. Forum* **2003**, *440–441*, 237–244. [CrossRef]
9. Duboc, M.; Magnier, V.; Brunel, J.F.; Dufrénoy, P. Experimental set-up and the associated model for squeal analysis. *Mech. Ind.* **2020**, *21*, 204. [CrossRef]
10. Bergman, F.; Eriksson, M.; Jacobson, S. The effect of reduced contact area on the occurrence of disc brake squeals for an automotive brake pad. *Proc. Inst. Mech. Eng. Part D J. Automob. Eng.* **2000**, *214*, 561–568. [CrossRef]
11. Xiang, Z.Y.; Mo, J.L.; Ouyang, H.; Massi, F.; Tang, B.; Zhou, Z.R. Contact behaviour and vibrational response of a high-speed train brake friction block. *Tribol. Int.* **2020**, *152*, 106540. [CrossRef]
12. Hetzler, H.; Willner, K. On the influence of contact tribology on brake squeal. *Tribol. Int.* **2012**, *46*, 237–246. [CrossRef]
13. Bergman, F.; Eriksson, M.; Jacobson, S. Influence of disc topography on generation of brake squeal. *Wear* **1999**, *225–229*, 621–628. [CrossRef]
14. Sinou, J.J.; Jézéquel, L. Mode coupling instability in friction-induced vibrations and its dependency on system parameters including damping. *Eur. J. Mech. A/Solids* **2007**, *26*, 106–122. [CrossRef]
15. AbuBakar, A.R.; Ouyang, H. Wear prediction of friction material and brake squeal using the finite element method. *Wear* **2008**, *264*, 1069–1076. [CrossRef]
16. Belhocine, A.; Ghazaly, N.M. Effects of material properties on generation of brake squeal noise using finite element method. *Lat. Am. J. Solids Struct.* **2015**, *12*, 1432–1447. [CrossRef]
17. Hentati, N.; Kchaou, M.; Cristol, A.L.; Najjar, D.; Elleuch, R. Impact of post-curing duration on mechanical, thermal and tribological behavior of an organic friction material. *Mater. Des.* **2014**, *63*, 699–709. [CrossRef]
18. Godet, M. The third-body approach: A mechanical view of wear. *Wear* **1984**, *100*, 437–452. [CrossRef]
19. Dowson, D.; Taylor, C.; Childs, T.; Dalmaz, G.; Berthier, Y.; Flamand, L.; Georges, J.; Lubrecht, A. *The Third Body Concept: Interpretation of Tribological Phenomena*; Elsevier: Amsterdam, The Netherlands, 1996; Volume 31.
20. Denape, J. Third body concept and wear particle behavior in dry friction sliding conditions. *Key Eng. Mater.* **2015**, *640*, 1–12. [CrossRef]
21. Davin, E.; Cristol, A.L.; Brunel, J.F.; Wear, Y.D.; Brunel, J.F.; Desplanques, Y. Wear mechanisms alteration at braking interface through atmosphere modification. *Wear* **2019**, *426*, 1094–1101. [CrossRef]
22. Kchaou, M.; Lazim, A.R.M.; Hamid, M.K.A.; Bakar, A.R.A. Experimental studies of friction-induced brake squeal: Influence of environmental sand particles in the interface brake pad-disc. *Tribol. Int.* **2017**, *110*, 307–317. [CrossRef]
23. Tison, T.; Heussaff, A.; Massa, F.; Turpin, I.; Nunes, R.F. Improvement in the predictivity of squeal simulations: Uncertainty and robustness. *J. Sound Vib.* **2014**, *333*, 3394–3412. [CrossRef]
24. Kasem, H.; Bonnamy, S.; Berthier, Y.; Jacquemard, P. Characterization of surface grooves and scratches induced by friction of C/C composites at low and high temperatures. *Tribol. Int.* **2010**, *43*, 1951–1959. [CrossRef]
25. Lee, S.; Jang, H. Effect of plateau distribution on friction instability of brake friction materials. *Wear* **2018**, *400–401*, 1–9. [CrossRef]
26. Lai, V.V.; Paszkiewicz, I.; Brunel, J.F.; Dufrénoy, P. Multi-scale contact localization and dynamic instability related to brake squeal. *Lubricants* **2020**, *8*, 43. [CrossRef]
27. Deltombe, R.; Kubiak, K.J.; Bigerelle, M. How to select the most relevant 3D roughness parameters of a surface. *Scanning* **2014**, *36*, 150–160. [CrossRef]